Formulation of Modal Based Elements in Nonlinear, Flexible Multibody Dynamics*

Olivier A. Bauchau and Jesus Rodriguez.
School of Aerospace Engineering,
Georgia Institute of Technology,
Atlanta, GA, USA.

Abstract

This paper is concerned with the modeling of elastic components in nonlinear, flexible multibody systems. The behavior of the elastic components will be represented by a modal expansion, thereby greatly reducing the computational cost of the simulation. In this work, a floating frame approach is used. The total motion of the elastic body consists of the superposition of the rigid body motions of the floating frame and of elastic motions that are assumed to remain small. The proposed formulation makes use of a component mode synthesis technique that leaves the analyst free to choose any type of modal basis and simplifies the connection of the elastic components to other components of the system. The proposed formulation is independent of the finite element analysis package used to compute the modes of the elastic components. It is also shown that in the absence of elastic deformations, the formulation recovers the exact equations of motion for a rigid body.

1 Introduction

The study of multibody system dynamics has received considerable attention over the last thirty years as it enables the analysis and design of numerous systems such as ground, air and space transportation vehicles, manufacturing machines, manipulators and robots, and other complex mechanical systems. Multibody systems are composed of a variety of components including joints, and rigid and flexible bodies. The modeling of the elastic bodies is one of the most difficult aspects of multibody systems dynamics, and many different formulations have been presented in the literature. Comprehensive reviews of the state of the art are found in references [1] and [2].

One of the most common approaches to the modeling of flexible multibody systems is based on the concept of floating frames [1, 2]. The total motion of the flexible body is broken into two parts: rigid body motions represented by the motion of the floating frame, and superimposed "elastic motions". This decomposition allows the introduction of simplifying assumptions: although the total motion is always finite, the elastic motions may, in some cases, be assumed to give rise to infinitesimal deformations. Many problems of great practical importance fall in this category. Consider, for instance, road or rail vehicles: the body of the vehicle undergoes large rigid body motions but the elastic deformations remain small. Of course, this assumption is no longer valid during a crash: in that case, large plastic deformations will be encountered. It should also be noted that other components of the vehicle, such as the suspension, wheels, and tires are inherently of a nonlinear nature. Another example is that of a rotorcraft. Under normal operation, the fuselage

Journal of Multiscale Computational Engineering, **1**, No 2 & 3 pp 161 – 180, 2003.

undergoes large rigid body motions but small elastic deformations. During maneuvering flight, large rotations will be encountered. Here again, the other components of the rotorcraft, the main and tail rotor, and the landing gear, are inherently nonlinear.

In such case, it seems natural to use modal reduction techniques to represent the small elastic motions in an efficient manner. The system size will be considerably reduced, together with the resulting computational cost. In addition, since high frequency modes are eliminated, larger time step sizes can be used in the simulation. The focus of this paper is the formulation of modal based elements that can be used within the framework of finite element based, nonlinear flexible multibody dynamics formulations.

Although the concept of floating frame is rather intuitive, the implementation of a computational procedure based on this idea must deal with several thorny issues. First, the accuracy of the analysis will critically depend on the selection of a suitable modal basis. Second, a specific floating frame must be selected: it could be attached to a point of the elastic body or moving with respect to it. Third, the modal based elements should be easy to couple with the other components of the system modeled with multibody formulations. This points towards the use of component mode synthesis techniques that are well developed for structural dynamics problems. Fourth, in the absence of elastic deformations, the formulation should recover the exact equations of motion for a rigid body. Finally, the formulation should be independent of the finite element analysis package used to compute the modes of the elastic components. These various issues will be discussed in more detail in the following paragraphs.

The first critical step is the selection of a suitable modal basis. Ideally, the selected modes should capture as accurately as possible the deformation patterns encountered during operation. Consequently, the analyst should be given the greatest possible freedom to select the type of modes he sees fit. The formulation should not put any restriction on the choice of the modal basis. Several authors have addressed the mode selection process [3, 4, 5, 6, 7, 8, 9].

Next, a specific floating frame must be selected. Since there exits no unique manner of defining the "rigid" and "elastic" motions, the floating frame can be selected in a number of different ways. Several authors make use of body-attached frames, *i.e.* the floating frame is attached to an arbitrary point in the body [10, 6, 8]. Other authors rely on floating frames moving with respect to the elastic body [11, 9]. Since the choice of the location of the moving frame is not unique, a specific condition must be selected to remove this indeterminacy. For instance, one can choose to minimize the kinetic energy [11], or to place the frame at the mass center of the structure [9]. The choice of one condition or the other seems to be a matter of computational convenience. The moving frame approach seems to be more desirable than the body-attached approach because it eliminates the need to arbitrarily select a material point where to attach the floating frame. On the other hand, the moving frame approach also involves the analyst's insight since a specific condition must be selected to determine its location. Furthermore, this latter approach comes at the expense of additional computational complexity. In this work, a body-attached frame will be used.

In some formulations, the choice of the floating frame is intimately linked to that of the modes used in the reduction technique [12, 13, 1]. This linkage hinders the selection of the most appropriate modes because the boundary conditions used to compute them do not necessarily match those of the flexible component once it is part of a multibody system.

In the classical application of modal analysis [14], the displacement field is represented as a linear combination of modes shapes. This type of representation has been used by some authors [15] in the context of multibody dynamics analysis, but it requires special techniques for coupling the modal based element with the other components of the system. Typically, this is done by formulating a constraint condition that equates the modal superposition to the physical displacement at a node of the model [16]. However, this approach does not take advantage of the component mode synthesis techniques that have been developed for structural dynamics problems over the past thirty years. These techniques are aimed at computing the eigenmodes of very large structures in an efficient

manner. The complete structure is broken into a number of substructures whose eigenmodes are easily computed. The substructures are then connected together to yield a lower order model of the complete structure. Each substructure involves two types of degrees of freedom: physical degrees of freedom at a limited number of connection points (called "boundary nodes"), and modal degrees of freedom representing its internal flexibility. Clearly, the need to interconnect the substructures is an integral part of the reduction technique and seems therefore ideally suited to the present problem. Among the most widely used component mode synthesis techniques are those of Craig and Bampton [17], McNeal [18], Rubin [19]. Other efforts include those of Herting [20], Hintz [21], and refinements of the Craig-Bampton method [22].

Component mode synthesis methods were first used in the context of multibody dynamics by Haug and coworkers [4, 5, 23, 24], and later by Cardona and coworkers [6, 8, 9] who used the Craig-Bampton method. Unfortunately, this method requires the use of modes associated with clamped conditions at the boundary nodes, thereby limiting the analyst's freedom to select the most appropriate modal basis. Consequently, the modal basis might poorly approximate the elastic behavior of the component. This fundamental limitation of the approach was recognized by Craig and Bampton who suggested the use of "static correction modes" to alleviate the problem. It also prompted the development of the McNeal-Rubin method. However, in this case, free conditions must be used at all boundary nodes, limiting again the analyst's freedom. Furthermore, this method is more cumbersome to implement than the Craig-Bampton method; it seems that the McNeal-Rubin method has not been used in conjunction with multibody formulations. Finally, Herting's method offers a more general approach that enables the analyst to choose *any* type of modes. In fact, predictions based on the Craig-Bampton and McNeal-Rubin methods were found to be in good agreement with those obtained from Herting's method [20]. In this work, Herting's method will be used as it provides the analyst maximum flexibility in the choice of the modal basis. Furthermore, it allows independent choices to be made for the selection of the floating frame and of the modal basis.

The formulation of modal based elements should be independent of the finite element analysis package used to compute the modes of the elastic components [4, 5, 6, 8, 9]. This means that the computation of the mass and stiffness coefficients used for the formulation of a modal based element should be solely based on the information readily provided by the finite element package. Some formulations have been proposed in which the finite element analysis tool is embedded in the multibody formulation [25]. Although higher accuracy can be achieved in that manner, this is clearly not a practical option if a large dimensional finite element model is required for the representation of the elastic components. Yoo and Haug [4, 5] showed that by assuming a lumped mass representation of the elastic body, the modal based formulation could be fully decoupled from the finite element package. Unfortunately, the lumped mass approximation is rarely used in today's finite element models of complex structures. Cardona and Géradin [6, 8, 9] used a corotational techniques to achieve the same decoupling without resorting to the lumped mass approximation. The proposed approximation is fully independent of the finite element analysis package. The mass and stiffness coefficients of the modal based element are computed on the sole basis of the unconstrained mass and stiffness matrices of the elastic component and Herting's transformation. It is also shown that the same transformation applies to inertial velocities required to compute the kinetic energy of the elastic component, under the sole assumption of small displacements.

The goal of this paper is to present a modal reduction technique that can be coupled to nonlinear, flexible multibody system models. The proposed approach gives the analyst maximum freedom to chose any set of modes sees fit, in contrast with other available methods that require specific sets of modes to be selected. Both body attached or moving frames can be used. The modal element is readily coupled to the rest of the model without requiring special constraint elements; this is achieved by means of boundary nodes that retain physical degrees of freedom. The proposed approach is completely independent of the finite element package used to compute the modes of the

elastic structure.

The paper is organized in the following manner. After a brief discussion of the notational conventions used in this work, the component mode synthesis technique presented by Herting [20] is briefly reviewed in section 3. Section 4 then describes the modal based multibody formulation. Finally, section 5 presents numerical examples to validate the proposed formulation.

2 Notational Conventions

The kinematic description of bodies in their reference and deformed configurations will make use of three orthonormal bases. First, an inertial basis is used as a global reference for the system; it is denoted $\mathcal{I} := (\bar{\imath}_1, \bar{\imath}_2, \bar{\imath}_3)$. A second basis $\mathcal{B}^0 := (\bar{e}_{01}, \bar{e}_{02}, \bar{e}_{03})$, is attached to the body and defines its orientation in the reference configuration. Finally, a third basis $\mathcal{B} := (\bar{e}_1, \bar{e}_2, \bar{e}_3)$ defines the orientation of the body in its deformed configuration.

Let $\underline{u}_0$ and $\underline{u}$ be the displacement vectors from $\mathcal{I}$ to $\mathcal{B}^0$ and $\mathcal{B}^0$ to $\mathcal{B}$, respectively, and R_0 and R the rotation tensors from $\mathcal{I}$ to $\mathcal{B}^0$ and $\mathcal{B}^0$ to $\mathcal{B}$, respectively. In this work, all vector and tensor components are measured in either $\mathcal{I}$ or $\mathcal{B}$. For instance, the components of vector $\underline{u}$ measured in $\mathcal{I}$, and $\mathcal{B}$ will be denoted $\underline{u}$, and $\underline{u}^*$, respectively, and clearly

$$\underline{u}^* = (RR_0)^T \underline{u}. \tag{1}$$

Similarly, the components of tensor R measured $\mathcal{I}$ and $\mathcal{B}$ will be denoted R and R^*, respectively. The skew-symmetric matrix formed with the components $\underline{u}$ will be denoted $\tilde{u}$.

3 Herting's Transformation

Consider an elastic component whose linearized equations of motion are in the following form

$$M\ddot{\underline{\hat{u}}}^* + K\underline{\hat{u}}^* = \underline{\hat{F}}(t), \tag{2}$$

where $\underline{\hat{u}}^*(t)$ is the array of nodal displacements and rotations, $\underline{\hat{F}}(t)$ the array of externally applied nodal forces, K and M the unconstrained stiffness and mass matrices of the component, respectively, and t time. For three dimensional problems, matrix K is six times singular, corresponding to the six rigid body modes of the component. The structure is assumed to be undamped or lightly damped and hence, damping effects are neglected. Eqs. (2) form a large set of N algebraic equations, typically obtained from a spatial discretization process such as the finite element method. Let matrix P store all the mass normalized eigenmodes of the component in order of ascending frequencies

$$P = [P_R, P_E], \tag{3}$$

where $P_R = \left[\underline{u}_1, \underline{u}_2, \ldots \underline{u}_{N_R}\right]$ stores the N_R rigid body modes of the structure and $P_E = \left[\underline{u}_{N_R+1}, \underline{u}_{N_R+2}, \ldots \underline{u}_N\right]$ its $N - N_R$ elastic modes.

The aim of this work is to develop a modal approximation to the component represented by eqs. (2) which will be connected to others components to form the complete system to be analyzed. The other components could be modeled by a modal representation, or by a multibody formulation. In order to allow the connection of a specific component to others, its degrees of freedom will be partitioned into boundary and interior degrees of freedom, denoted $\underline{d}^{B*}$ and $\underline{\hat{u}}^{I*}$, respectively. The array $\underline{d}^{B*T} = \lfloor \underline{d}_1^{B*T}, \underline{d}_2^{B*T}, \ldots \underline{d}_m^{B*T} \rfloor$ stores the six degrees of freedom for each of the m boundary points of the component. Each boundary point requires six degrees of freedom, three displacements

and three rotations, for compatibility with multibody formulations, *i.e.* $\underline{d}_i^{B*T} = \lfloor \underline{u}_i^{B*T}, \underline{\theta}_i^{B*T} \rfloor$. The following partition of the structural matrices is performed

$$M = \begin{bmatrix} M^{BB} & M^{BI} \\ M^{IB} & M^{II} \end{bmatrix}; \quad K = \begin{bmatrix} K^{BB} & K^{BI} \\ K^{IB} & K^{II} \end{bmatrix}, \tag{4}$$

$$\underline{\hat{u}}^* = \begin{bmatrix} \underline{d}^{B*} \\ \underline{\hat{u}}^{I*} \end{bmatrix}; \quad \underline{\hat{F}}(t) = \begin{bmatrix} \underline{F}^B(t) \\ \underline{\hat{F}}^I(t) \end{bmatrix}, \tag{5}$$

and

$$P_R = \begin{bmatrix} P_R^B \\ P_R^I \end{bmatrix}; \quad P_E = \begin{bmatrix} P_E^B \\ P_E^I \end{bmatrix}, \tag{6}$$

where the superscripts $(\cdot)^B$ and $(\cdot)^I$ denoted the boundary and interior degrees of freedom, respectively. It is assumed that the partition K^{II} is nonsingular.

Herting [20] introduced a coordinate transformation

$$\underline{\hat{u}}^* = H_H \, \underline{\bar{u}}, \tag{7}$$

defined by a set of shape functions H_H

$$H_H = \begin{bmatrix} I & 0 & 0 \\ G^{IB} & H_R^I & P_E^I - G^{IB} P_E^B \end{bmatrix}, \tag{8}$$

where

$$G^{IB} = -K^{II-1} K^{IB}, \tag{9}$$

$$H_R^I = -K^{II-1} \left(M^{IB} + M^{II} G^{IB} \right) P_R^B. \tag{10}$$

The reduced set of degrees of freedom is

$$\underline{\bar{u}}^T = \lfloor \underline{d}^{B*T}, \; \underline{q}_R^T, \; \underline{q}_E^T \rfloor, \tag{11}$$

where $\underline{q}_R$ and $\underline{q}_E$ correspond to the modal participation factors for the rigid and elastic modes, respectively.

In the absence of interior loads, *i.e.* when $\underline{\hat{F}}^I(t) = 0$, the equations of motion, eqs. (2), reduce to

$$\bar{M} \, \underline{\ddot{\bar{u}}} + \bar{K} \, \underline{\bar{u}} = \underline{\bar{F}}, \tag{12}$$

where

$$\bar{M} = H_H^T M H_H; \quad \bar{K} = H_H^T K H_H; \quad \underline{\bar{F}} = H_H^T \underline{\hat{F}}(t). \tag{13}$$

Typically, boundary degrees of freedom and modal coordinates are coupled in the reduced mass matrix $\bar{M}$, whereas the reduced stiffness matrix takes the following form

$$\bar{K} = \begin{bmatrix} \bar{K}^{BB} & 0 \\ 0 & \bar{K}^{qq} \end{bmatrix}, \tag{14}$$

where $\bar{K}^{BB}$ is the partition obtained from a Guyan reduction and the superscript $(.)^q$ refers to the modal coordinates. Clearly, boundary degrees of freedom and modal coordinates are statically uncoupled.

4 Multibody Formulation

In this section, the kinematics of the modal based element are presented. The proposed formulation follows the floating frame approach, where small elastic displacements and rotations are superimposed to the large rigid body motion of the elastic body. Expressions for the kinetic and strain energies are then derived.

4.1 Modal based element kinematics

Consider the elastic body shown in fig. 1. The overall rigid body motion of the elastic body is described by a floating frame whose orientation is defined by the orthonormal bases $\mathcal{B}^{0F} := \left(\bar{e}^F_{01}, \bar{e}^F_{02}, \bar{e}^F_{03}\right)$ and $\mathcal{B}^F := \left(\bar{e}^F_1, \bar{e}^F_2, \bar{e}^F_3\right)$ in the reference and deformed configurations, respectively. Similarly, two additional orthonormal bases define the orientation of a frame rigidly attached to the body at an arbitrary point $\mathbf{P}$, $\mathcal{B}^{0P} := \left(\bar{e}^P_{01}, \bar{e}^P_{02}, \bar{e}^P_{03}\right)$ and $\mathcal{B}^P := \left(\bar{e}^P_1, \bar{e}^P_2, \bar{e}^P_3\right)$ in the reference and deformed configurations, respectively. R^F_0 and R^F are the components of the rotation tensors from the inertial frame $\mathcal{I}$ to $\mathcal{B}^{0F}$ and $\mathcal{B}^{0F}$ to $\mathcal{B}^F$, respectively, both measured in $\mathcal{I}$. Similarly, R^P_0 and R^P are the components of the rotation tensors from $\mathcal{I}$ to $\mathcal{B}^{0P}$ and $\mathcal{B}^{0P}$ to $\mathcal{B}^P$, respectively, both measured in $\mathcal{I}$. In the reference configuration, the origin of the floating and body-attached frames are denoted by $\underline{x}^F_0$ and $\underline{x}^P_0$, respectively. The position vector $\underline{s}^P$ of point $\mathbf{P}$ with respect to the floating frame vector is $\underline{s}^P = \underline{x}^P_0 - \underline{x}^F_0$. The orientations of the floating and body-attached frames are identical in the reference configuration, *i.e.* $R^F_0 = R^P_0 = R_0$. The displacement vectors of the floating and body-attached frames are denoted $\underline{x}^F$ and $\underline{x}^P$, respectively.

The total motion of the elastic body consists of the superposition of a rigid body motion and an elastic motion. The rigid body motion, defined by the motion of the floating frame, brings the elastic body to the "fictitious rigid body configuration" shown in fig. 1. Since this motion is rigid, the position vector of point $\mathbf{P}$ with respect to the floating frame, measured in this frame, remains unchanged, *i.e.* $\underline{s}^{P*} = \underline{S}^{P*}$, where $\underline{s}^{P*} = R^T_0\,\underline{s}^P$, $\underline{S}^{P*} = (R^F R_0)^T\,\underline{S}^P$, and $\underline{S}^P$ denotes the position vector of point $\mathbf{P}$ in the fictitious rigid body configuration. The position of point $\mathbf{P}$ is now written as

$$\underline{x}^P_0 + \underline{x}^P = \underline{x}^F_0 + \underline{x}^F + \underline{S}^P + \underline{u}^P = \underline{x}^F_0 + \underline{x}^F + (R^F R_0)(\underline{s}^{P*} + \underline{u}^{P*}), \tag{15}$$

where $\underline{u}^P$ is the elastic displacement of the body, and $\underline{u}^{P*} = (R^F R_0)^T\,\underline{u}^P$ the components of this displacement vector measured in frame $\mathcal{B}^F$. Solving eq. (15) then yields

$$\underline{u}^{P*} = (R^F R_0)^T \left(\underline{x}^P_0 + \underline{x}^P - \underline{x}^F_0 - \underline{x}^F\right) - \underline{s}^{P*}. \tag{16}$$

In general, the elastic body also undergoes elastic rotations that will be defined in the following manner

$$\underline{\theta}^{P*} = \frac{1}{2}\begin{bmatrix} g_{32} - g_{23} \\ g_{13} - g_{31} \\ g_{21} - g_{12} \end{bmatrix} = \frac{1}{2}\begin{bmatrix} R^*_{32} - R^*_{23} \\ R^*_{13} - R^*_{31} \\ R^*_{21} - R^*_{12} \end{bmatrix} = \bar{n}^*\ \sin\phi, \tag{17}$$

where R^*_{ij} are the components of the relative rotation tensor $R^* = (R^F R_0)^T R^P R_0$; ϕ the magnitude of this relative rotation; $\bar{n}^*$ the unit vector about which it takes place; and $g_{\alpha\beta} = \bar{e}^{FT}_\alpha\ \bar{e}^P_\beta$. If the elastic displacements remain small, $\underline{\theta}^{P*} \approx \bar{n}^*\,\phi$ represents the infinitesimal rotation vector, although R^P and R^F both are finite rotations.

Since eqs. (16) and (17) are valid for any point on the elastic body, they also hold for the boundary points, hence

$$\underline{u}^{B*} = (R^F R_0)^T \left(\underline{x}^B_0 + \underline{x}^B - \underline{x}^F_0 - \underline{x}^F\right) - \underline{s}^{B*}, \tag{18}$$

and

$$\underline{\theta}^{B*} = \frac{1}{2}\begin{bmatrix} g_{32} - g_{23} \\ g_{13} - g_{31} \\ g_{21} - g_{12} \end{bmatrix}, \tag{19}$$

where $g_{\alpha\beta} = \bar{e}^{FT}_\alpha\ \bar{e}^B_\beta$.

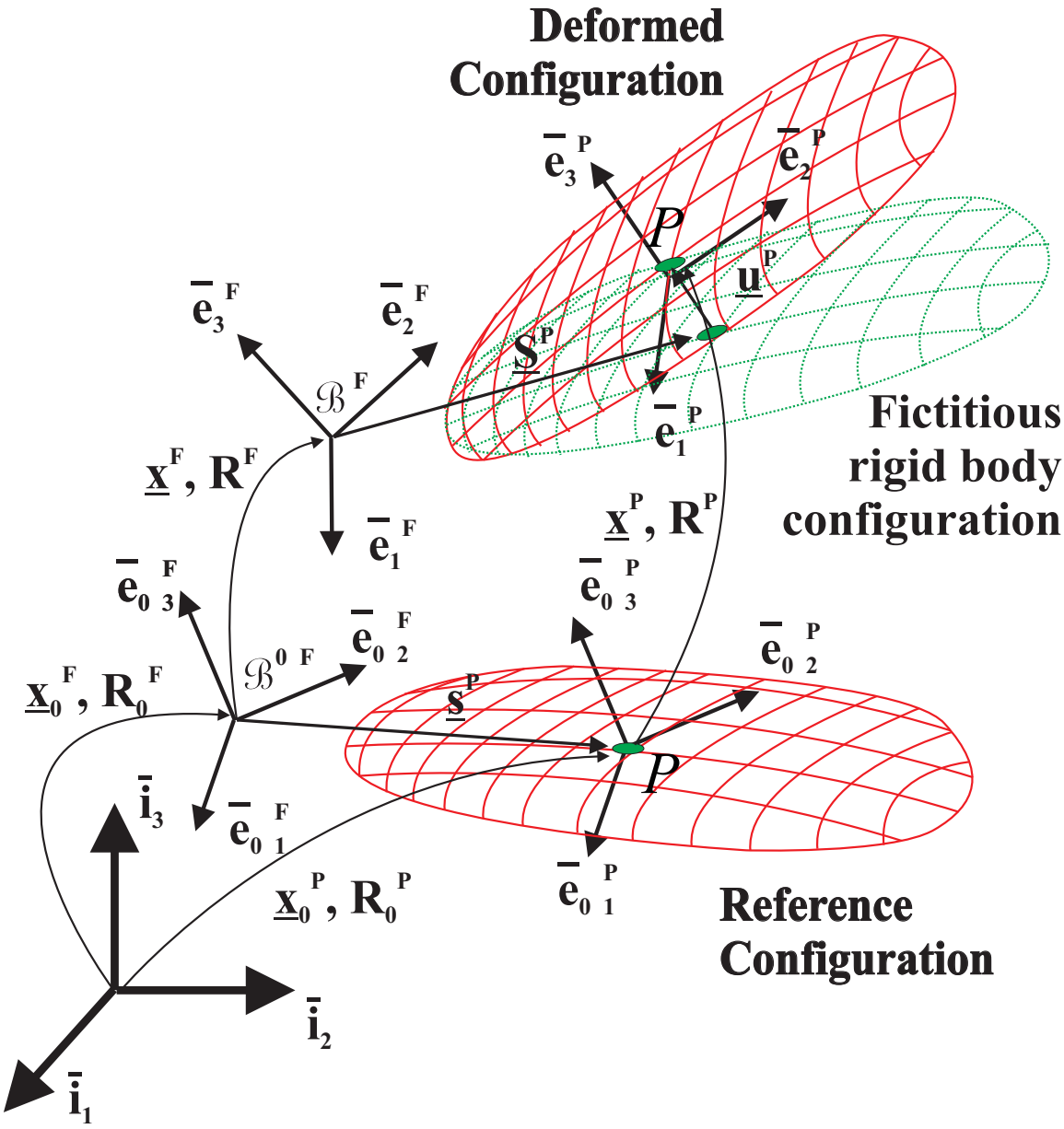

Figure 1: Configuration of the elastic body.

4.2 Strain Energy

With the help of Herting's transformation, eq. (7), the strain energy of the elastic body can be written as $\mathcal{V} = 1/2\ \underline{\bar{u}}^T \bar{K}\, \underline{\bar{u}}$. Using eqs. (18) and (19), the elastic forces $\underline{\mathcal{F}}^e$ are then readily found as

$$\delta\mathcal{V} = \begin{bmatrix} \underline{\delta x}^F \\ \underline{\delta\psi}^F \\ \underline{\delta x}^B \\ \underline{\delta\psi}^B \\ \underline{\delta q} \end{bmatrix}^T \begin{bmatrix} - & R^F R_0\ \underline{f}^u \\ - & T\ \underline{f}^\theta - \tilde{u}\, R^F R_0\ \underline{f}^u \\ & R^{\overline{F}} R_0\ \underline{f}^u \\ & T\ \underline{f}^\theta \\ & \underline{f}^q \end{bmatrix} = \begin{bmatrix} \underline{\delta x}^F \\ \underline{\delta\psi}^F \\ \underline{\delta x}^B \\ \underline{\delta\psi}^B \\ \underline{\delta q} \end{bmatrix}^T \underline{\mathcal{F}}^e, \tag{20}$$

where

$$\begin{bmatrix} \underline{f}^u \\ \underline{f}^\theta \\ \underline{f}^q \end{bmatrix} = \bar{K} \begin{bmatrix} \underline{u}^{B*} \\ \underline{\theta}^{B*} \\ \underline{q} \end{bmatrix} \tag{21}$$

are elastic force components, and

$$\underline{q} = \begin{bmatrix} \underline{q}_R \\ \underline{q}_E \end{bmatrix}, \tag{22}$$

the array of modal participation factors. The following notations were introduced: $\underline{u} = \underline{x}_0^B + \underline{x}^B - \underline{x}_0^F - \underline{x}^F$; $T = 1/2\ [\underline{h}_{32} - \underline{h}_{23},\ \underline{h}_{13} - \underline{h}_{31},\ \underline{h}_{21} - \underline{h}_{12}]$, and $\underline{h}_{\alpha\beta} = \tilde{e}_\alpha^F\ \bar{e}_\beta^B$.

For simplicity of the exposition, the formulation was presented here for a single boundary point. The case of multiple boundary point is obtained by a straightforward generalization. The evaluation of the strain energy of the modal based element only requires the reduced stiffness matrix $\bar{K} = H_H^T K H_H$; hence, it is independent of the finite element code used to model the elastic component.

4.3 Kinetic Energy

The total kinetic energy of the elastic body $\mathcal{K}$ is given by

$$\mathcal{K} = \frac{1}{2} \int_V \underline{\dot{x}}^{P*T}\, \underline{\dot{x}}^{*P}\, \rho \mathrm{d}V, \tag{23}$$

where $\dot{(.)} = \mathrm{d}(.)/\mathrm{dt}$; ρ is the material density, and V the volume of the elastic body. For eq. (15), the inertial velocity, $\underline{\dot{x}}^P$, of an arbitrary point of the elastic body is

$$\underline{\dot{x}}^P = \underline{\dot{x}}^F + (\dot{R}^F R_0)\, (\underline{s}^{P*} + \underline{u}^{P*}) + (R^F R_0)\, \underline{\dot{u}}^{P*}. \tag{24}$$

Since the elastic displacements $\underline{u}^{P*}$ are assumed to remain small, this velocity is approximated by

$$\underline{\dot{x}}^P = \underline{\dot{x}}^F + (\dot{R}^F R_0)\, \underline{s}^{P*} + (R^F R_0)\, \underline{\dot{u}}^{P*}, \tag{25}$$

and its components measured in the floating frame become

$$\underline{\dot{x}}^{P*} = (R^F R_0)^T \underline{\dot{x}}^P = (R^F R_0)^T \underline{\dot{x}}^F + \tilde{\omega}^{F*} \underline{s}^{P*} + \underline{\dot{u}}^{P*} = \underline{v}_R^* + \underline{\dot{u}}^{P*}, \tag{26}$$

where $\underline{\omega}^{F*}$ is the angular velocity of the floating frame. The total velocity field is the superposition of the "rigid velocity" due to the floating frame motion, and the "elastic velocity", $\underline{\dot{u}}^{P*}$. This velocity field is now discretized in terms of nodal values $\underline{\hat{v}}^*$ with the help of interpolation functions

$$\underline{\dot{x}}^{P*} = H\, \underline{\hat{v}}^*, \tag{27}$$

where the matrix H stores the classical, finite element shape function [26]. The kinetic energy now becomes

$$\mathcal{K} = \frac{1}{2}\,\underline{\hat{v}}^{*T}\left[\int_V H^T H\,\rho \mathrm{d}V\right]\underline{\hat{v}}^{*} = \frac{1}{2}\,\underline{\hat{v}}^{*T} M \underline{\hat{v}}^{*}, \tag{28}$$

where M is the mass matrix of the elastic component, see eqs. (2).

Next, taking a time derivative of Herting's transformation, eq. (7), leads to

$$\begin{bmatrix} \underline{\dot{d}}^{B*} \\ \underline{\dot{\hat{u}}}^{I*} \end{bmatrix} = \begin{bmatrix} I & 0 \\ G^{IB} & H^{Iq} \end{bmatrix} \begin{bmatrix} \underline{\dot{d}}^{B*} \\ \underline{\dot{q}} \end{bmatrix}, \tag{29}$$

where $H^{Iq} = \left[H^I_R,\ P^I_E - G^{IB}P^B_E\right]$.

Consider now an array of nodal displacements, $\underline{\hat{u}}^*_R$, storing a rigid body mode of the elastic component. Partition (4) then implies $K^{IB}\,\underline{d}^{B*}_R + K^{II}\,\underline{\hat{u}}^{I*}_R = 0$, and hence $\underline{\hat{u}}^{I*}_R = G^{IB}\,\underline{d}^{B*}_R$ for any of the six rigid body modes. If the elastic component features a single boundary point, G^{IB} can be interpreted as storing the value of rigid body motion at the interior points the elastic component. Elementary kinematics for a rigid body then imply

$$\underline{\hat{v}}^{I*}_R = G^{IB}\,\underline{v}^{B*}_R, \tag{30}$$

where $\underline{\hat{v}}^{I*}_R$ and $\underline{v}^{B*}_R = \underline{\hat{v}}^{B*}_R$ are the rigid components of velocity at the interior and boundary nodes, respectively. Adding this relationship to eq. (29) then yields

$$(\underline{\hat{v}}^{I*}_R + \underline{\dot{\hat{u}}}^{I*}) = G^{IB}\,(\underline{v}^{B*}_R + \underline{\dot{d}}^{B*}) + H^{Iq}\,\underline{\dot{q}}. \tag{31}$$

In view of eq. (26), the terms between the first and second sets of parentheses represent the total velocity of an interior and boundary point, respectively. It follows that Herting's transformation, eq. (29), can be recast as

$$\begin{bmatrix} \underline{v}^{B*} \\ \underline{\hat{v}}^{I*} \end{bmatrix} = H_H \begin{bmatrix} \underline{v}^{B*} \\ \underline{\dot{q}} \end{bmatrix}. \tag{32}$$

If the elastic component features more than one boundary point, it can be readily shown that this relationship still holds, provided that the elastic motions at the boundary points remain small. Note the close parallel between Herting's transformation for displacements and velocities, eqs. (7) and (32), respectively. Although Herting's transformation, eq. (7), is a linearized relationship inherently associated with the small displacement assumption, the corresponding transformation for velocities, eq (32), is valid for total velocities (involving both small "elastic" and large "rigid" velocities), under the same small displacement assumption.

Using eq. (32), the kinetic energy of the components, eq. (28), becomes

$$\mathcal{K} = \frac{1}{2}\begin{bmatrix} \underline{v}^{B*} \\ \underline{\dot{q}} \end{bmatrix}^T \bar{M} \begin{bmatrix} \underline{v}^{B*} \\ \underline{\dot{q}} \end{bmatrix}. \tag{33}$$

The inertial forces $\underline{\mathcal{F}}^i$ are readily found from variations of the kinetic energy

$$\delta\mathcal{K} = \begin{bmatrix} \delta\underline{x}^B \\ \delta\underline{\psi}^B \\ \hline \delta\underline{q} \end{bmatrix}^T \begin{bmatrix} (R^B R_0\,\underline{h}^*)^{\cdot} \\ (R^B R_0\,\underline{g}^*)^{\cdot} + \tilde{\dot{x}}^B R^B R_0\,\underline{h}^* \\ \underline{\dot{h}}^q \end{bmatrix} = \begin{bmatrix} \delta\underline{x}^B \\ \delta\underline{\psi}^B \\ \hline \delta\underline{q} \end{bmatrix}^T \underline{\mathcal{F}}^i, \tag{34}$$

where

$$\begin{bmatrix} \underline{h}^* \\ \underline{g}^* \\ \underline{h}^q \end{bmatrix} = \bar{M} \begin{bmatrix} \underline{v}^*_B \\ \underline{\omega}^*_B \\ \underline{\dot{q}} \end{bmatrix}, \tag{35}$$

are the momenta components.

Consider an elastic component featuring a single boundary point. If no modes are selected in Herting's transformation, the component is effectively modeled as a rigid body. The reduced mass matrix becomes

$$\bar{M} = \begin{bmatrix} I \\ G^{IB} \end{bmatrix}^T M \begin{bmatrix} I \\ G^{IB} \end{bmatrix} = M_{RR}. \tag{36}$$

Since in this case G^{IB} stores the value of rigid body motion at the interior points the component, M_{RR} becomes the exact 6×6 mass matrix for the rigid body. In other words, the formulation exactly reproduces rigid body dynamics when elasticity of the component is inhibited. Note that when more than one boundary point is used, elasticity is inherent to the formulation, even when no elastic modes are selected.

The evaluation of the kinetic energy of the modal based element only requires the reduced mass matrix $\bar{M} = H_H^T M H_H$; hence, it is independent of the finite element code used to model the elastic component.

4.4 Discretization of the elastic and inertial forces

Due to the complex dynamical behavior of multibody systems, it is desirable to used robust time integration methods [27, 28] that present nonlinear unconditional stability characteristics. Let t_i and t_f denote the initial and final instants of a time step, respectively. The subscripts $(\cdot)_i$ and $(\cdot)_f$ then indicate the value of a specific quantity at times t_i and t_f, respectively. The following discretization of the elastic forces is proposed

$$\underline{\mathcal{F}}^e_m = \begin{bmatrix} - & R^F_m R_0 \, \underline{f}^u_m \\ - & T_m \, \underline{f}^\theta_m - \tilde{u}_m \, R^F_m R_0 \, \underline{f}^u_m \\ & R^F_m R_0 \, \underline{f}^u_m \\ & T_m \, \underline{f}^\theta_m \\ & \underline{f}^q_m \end{bmatrix}, \tag{37}$$

where the subscript $(\cdot)_m = 1/2\,[(\cdot)_i + (\cdot)_f]$ indicates an averaged quantity, *e.g.* $R^F_m = (R^F_f + R^F_i)/2$. $T_m = 1/2\,[\underline{h}_{32m} - \underline{h}_{23m},\ \underline{h}_{13m} - \underline{h}_{31m},\ \underline{h}_{21m} - \underline{h}_{12m}]$ where $\underline{h}_{\alpha\beta m} = \tilde{e}^F_{\alpha m}\, \underline{e}^B_{\beta m}$. The following discretization of the inertial forces is proposed

$$\underline{\mathcal{F}}^i_m = \frac{1}{\Delta t} \begin{bmatrix} (R^B R_0 \, \underline{h}^*)_f - (R^B R_0 \, \underline{h}^*)_i \\ (R^B R_0 \, \underline{g}^*)_f - (R^B R_0 \, \underline{g}^*)_i + (\tilde{x}^B_f - \tilde{x}^B_i)\left(R^B R_0 \, \underline{h}^*\right)_m \\ \underline{h}^q_f - \underline{h}^q_i \end{bmatrix}, \tag{38}$$

where $\Delta t = t_f - t_i$. It is then readily shown that the work done by the elastic forces during one time step is $\Delta\mathcal{W}^e = \mathcal{V}_f - \mathcal{V}_i$, and that the work done by the inertial forces is $\Delta\mathcal{W}^i = \mathcal{K}_f - \mathcal{K}_i$. Consequently, in the absence of external loads, the equations of motion of the modal element imply $\mathcal{E}_f = \mathcal{K}_f + \mathcal{V}_f = \mathcal{K}_i + \mathcal{V}_i = \mathcal{E}_i$, *i.e.* the total mechanical $\mathcal{E}$ energy of the system is preserved. This energy preservation guarantees nonlinear unconditional stability of the time integration process and it can be readily extended to an energy decaying formulation by following the steps outlined in section 4.3 of [27].

4.5 Choice of the floating frame

The strain and kinetic energies of the modal based element were developed in sections 4.2 and 4.3 for a general kinematic configuration that involves a floating frame. Note that the floating frame explicitly appears in the expression of the strain energy, but not in that of the kinetic energy.

In order to implement the proposed formulation, a specific floating frame must be selected. The easiest choice is to attach the floating frame at a boundary point. This is readily achieved by Boolean identification of the corresponding degrees of freedom in the expression of the elastic forces, eq. (20). The inertial forces derived in eq. (34) can be used without modification. For a moving floating frame, the location and orientation of the floating frame become a function of the other degrees of freedom of the model, and hence, are eliminated from the formulation [8].

5 Numerical Examples

The following examples validate the proposed formulation. In all the examples a body-attached floating frame was used.

5.1 Validation Example

References [6] and [24] describe a computational example that demonstrates the use of modal based elements in mechanism analysis. In this proposed example, the root angular displacement ϕ of a flexible beam is prescribed to be the following function of time

$$\phi = \begin{cases} \frac{\omega_0}{T_0}\left[\frac{1}{2}\,t^2 + (\frac{T_0}{2\pi})^2(\cos\frac{2\pi t}{T_0} - 1)\right], & t \le T_0, \\ \omega_0(t - \frac{T_0}{2}), & t > T_0, \end{cases} \tag{39}$$

where $T_0 = 15$ sec. The physical properties of the beam can be found in ref. [24]. A constant time step $\Delta t = 2 \times 10^{-03}$ sec was used for all simulations.

Three cases were considered, denoted *case 0* to *2*, respectively. For *case 0*, the baseline case, the structure was modeled with three quadratic beam elements and the dynamic response was predicted without resorting to a modal reduction. In *case 1*, the linearized mass and stiffness matrices were computed from the finite element model and the proposed formulation was used to reduce the system. A single boundary point was used at the root of the beam and the body-attached floating frame was located there. The modal basis consists of two bending modes with fixed-free boundary conditions. *Case 2* is identical to *case 1*, but its modal basis consisted of three rigid body modes and two bending modes with free-free boundary conditions. It should be noted that the proposed formulation, because it is based on Herting's transformation, allows the use of both modal bases within the same computational procedure.

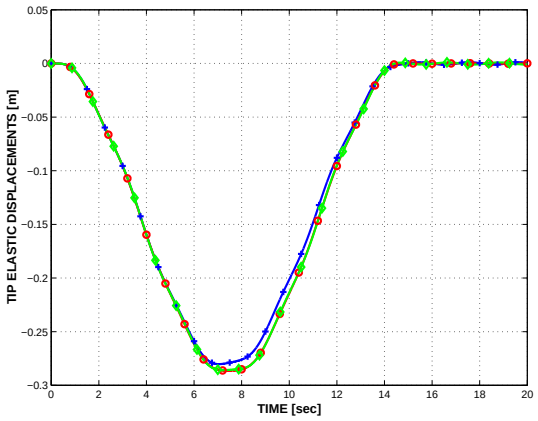

Figure 2: Time history of the transverse elastic tip displacements for $\omega_0 = 2.0$ rad/sec. *Case 0*: (+); *case 1*: (○); *case 2*: (◇).

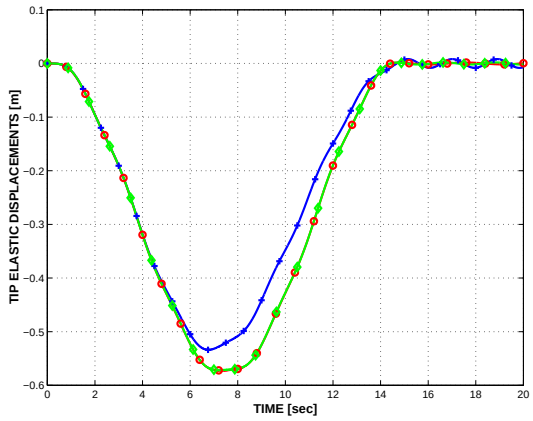

Figure 3: Time history of the transverse elastic tip displacements for $\omega_0 = 4.0$ rad/sec. *Case 0*: (+); *case 1*: (○); and *case 2*: (◇).

Revolute Joint at	M_0 [N.m]	ϕ_0 [rad]	n	μ [N.m.sec/rad]
A_1	2.0	$\pi/2$	6	20.0
B_1	1.6	π	12	9.0
B_2	1.4	π	12	7.0
B_3	1.0	π	12	5.0

Table 1: Physical properties of the springs and dampers at the revolute joints.

Fig. 2 shows the time history of the transverse elastic tip displacements for $\omega_0 = 2$ rad/sec. Clearly, the agreement between the predictions of the full finite element simulation and the reduced models is excellent. It is remarkable to observe the good correlation between *cases 1* and *2* although the selected modal bases were of a very different nature. Fig. 3 depicts the time history of the tip transverse elastic displacements when $\omega_0 = 4$ rad/sec. The agreement between the finite element solution and the reduced models is not as good because the higher angular velocity increases nonlinear effects. Correlation between cases *cases 1* and *2* remains excellent despite the different modal bases. For larger angular velocities, $\omega_0 > 4$ rad/sec, the response becomes unstable for the present linearized modal formulation, as also reported in refs. [6] and [24].

5.2 Deployment of a Space Antenna

The second example deals with the space antenna depicted in fig. 4. The antenna consists of four 5×5 m panels attached together by connector beams and revolute joints at points $\mathbf{A}_i$ and $\mathbf{B}_i$, respectively. The relative rotations at the revolute joints are denoted ϕ_i.

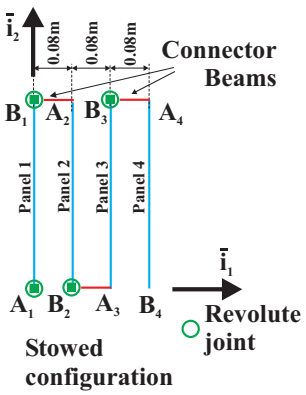

Figure 4: Configuration of the space antenna.

The motion of the antenna is nearly two-dimensional as the panels undergo very limited chord-wise deformation. Hence, the four panels were modeled as beams with the following properties: axial stiffness $EA = 290.0$ MN, bending stiffness $EI = 58.3$ N.m^2, shearing stiffness $GK = 31.2$ MN, mass per unit span $m = 18.75$ kg/m, and mass moment of inertia per unit span $I = 2.4$ mg.m. The connector beam properties were: axial stiffness $EA = 112.0$ MN, bending stiffness $EI = 37.3$ kN.m^2, shearing stiffness $GK = 35.9$ MN, mass per unit span $m = 5.6$ kg/m, and mass moment of inertia per unit span $I = 0.19$ g.m. Each of the eight revolute joints weighs 8 kg and is spring loaded to deploy the antenna. Each spring applies a moment $M_s = M_0[1 - (\phi/\phi_0)^n]$ at the joint. Furthermore, a damper is present in each joint and applies a moment $M_d = \mu\dot{\phi}$. The constants M_0, ϕ_0, n and μ are listed in table 1 for each joint. Under the effect of the springs in the revolute joint, the antenna deploys. A constant time step $\Delta t = 0.1$ sec was used for all simulations.

Several cases were considered, denoted *case 0* to *3*. For *case 0*, the baseline case, each of panel was modeled with four quadratic elements, and the dynamic response of the system was predicted without resorting to a modal reduction. In *case 1*, the proposed formulation was used. Two boundary nodes, located at the root point $\mathbf{A}_i$ and tip point $\mathbf{B}_i$, were kept for each beam. The body-attached frame was located at the root point $\mathbf{A}_i$ of each beam. The modal basis consisted of three bending modes with fixed-free boundary conditions. *Case 2* is identical to *case 1*, but its modal basis consisted of three bending modes with fixed-fixed boundary conditions. In *case 3* the

modal basis consisted of six modes: three rigid body modes and three bending modes with free-free boundary conditions. Adding more modes to the different modal bases did not significantly affect the predictions.

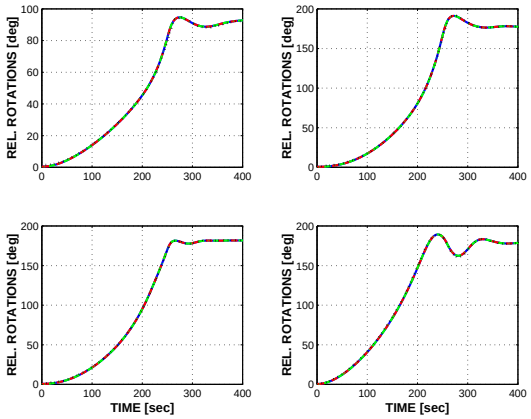

Figure 5: Relative rotation at the revolute joints. Joint at point A_1: top-left, B_1: top-right, B_2: bottom-left, and B_3: bottom-right figure. *Case 0*: solid line; *case 1*: dashed line; *case 2*: dashed-dotted line; and *case 3*: dotted line.

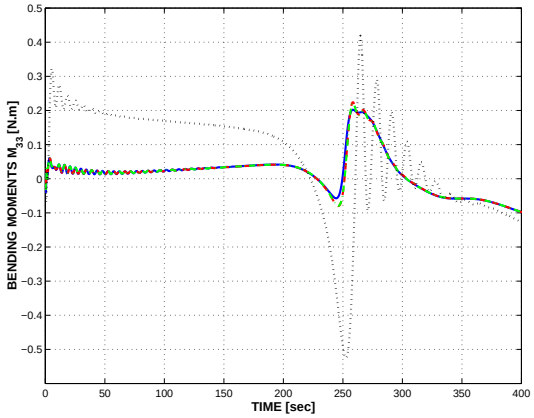

Figure 6: Mid-span bending moment M_{33} for *case 0*: solid line; *case 1*: dashed line; and *case 2*: dashed-dotted line.

In a first set of simulations, the spring stiffness constants M_0 at each of the revolute joints were reduced by a factor of four from their nominal values listed in table 1. Fig. 5 shows the relative rotations at each of the revolute joints. Excellent agreement is observed, despite of different modal bases used in each case. Fig. 6 depicts the mid-span bending moment M_{33} in the first panel. *Cases 1* and *2* show good correlation with the full finite element computation, whereas significant discrepancies are observed for *case 3*. Clearly, the use of free-free modes is not desirable for this particular problem, and the analyst should have complete freedom to select the most appropriate modal basis without modifying the formulation.

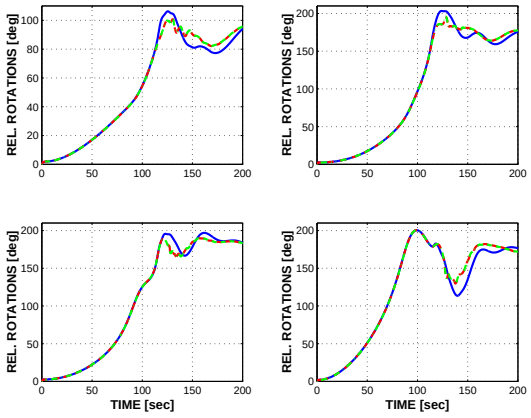

Figure 7: Relative rotation at the revolute joints. Joint at point A_1: top-left, B_1: top-right, B_2: bottom-left, and B_3: bottom-right figure. *Case 0*: solid line; *case 1*: dashed line; and *case 2*: dashed-dotted line.

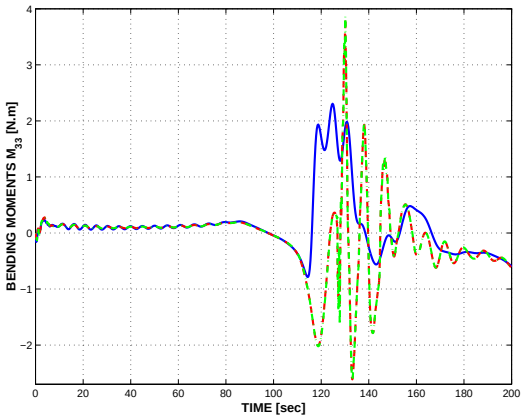

Figure 8: Mid-span bending moment M_{33} for *case 0*: solid line; *case 1*: dashed line; and *case 2*: dashed-dotted line.

In the second set of simulations, the spring stiffness constants listed in table 1 were used. *Case 3* was not run, in view of the poor performance of its modal basis. Due to the increased driving force,

the antenna deployed more rapidly and nonlinear effects, such stiffening of the panels due to axial forces, became more important. Fig. 7 depicts the relative rotations at each of the revolute joints. The finite element and reduced model solutions are in good agreement up to $t \approx 115$ sec. At this time, the four beams are nearly aligned to form the complete antenna, and vibrations of increased amplitude are observed. The same behavior can be observed in fig. 8 which depicts the time history of the mid-span bending moments M_{33} in the first panel. Here again, the predictions of all three cases are in good correlation up to $t \approx 115$ sec. At subsequent time, significant discrepancies are observed between the predictions of the full finite element models and those based on modal reduction techniques. The peak bending moments are grossly overestimated by the modal based models that cannot capture the stiffening of the panels in the presence of axial forces.

5.3 Crank-Panel Mechanism

The last example deals with the crank-panel mechanism shown in fig. 9. The mechanism consists of a 1×1 m panel connected to two reinforcing beams along the opposite edges **AD** and **BC**. The reinforcing beam along edge **AD** is connected to the ground by means of two revolute joints at points **A** and **D**, respectively. A spherical joint connects the other reinforcing beam to a push rod at point **B**. In turns, the push rod is connected to a crank by means of a universal joint at point **E**. Finally, a revolute joint connects the crank to the ground at point **O**, and the relative rotation at this joint is denoted ϕ. The mechanism is initially at rest and the root rotation of the crank is prescribed as

$$\phi(t) = \begin{cases} \pi/4\ (1 - \cos \pi t/T), & t \leq T, \\ \pi/2, & t > T, \end{cases} \qquad (40)$$

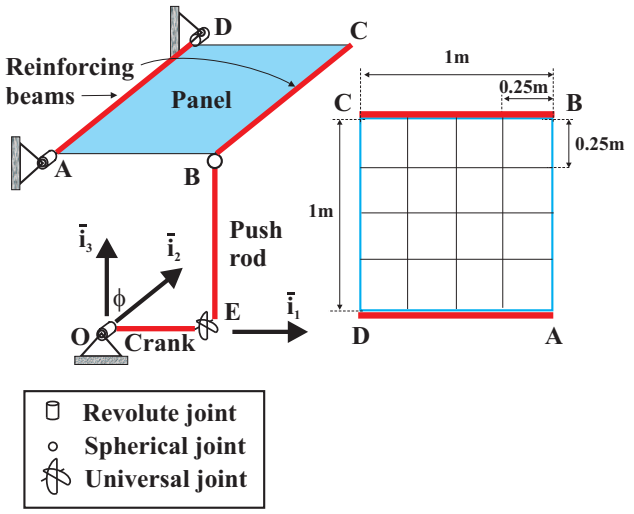

Figure 9: Configuration of the crank-panel mechanism.

The physical properties of the system were as follows: crank length $\ell_C = 0.25$ m, push rod length $\ell_P = 1.0$ m and panel thickness $h = 15$ mm. The entire mechanism is made of aluminum: Young's modulus $E = 73$ GPa, Poisson's ratio $\nu = 0.3$, and density $\rho = 2,700$ kg/m^3. All beams present square cross-sections: 40 ×40 mm for both the crank and push rod; 60×60 mm and 30×30 mm for the reinforcing beams along the **AD** and **BC** edges, respectively.

Several cases were considered. *Case 1A* is the baseline case where no modal reduction was performed. The panel was modeled with 16 quadratic shell elements [29] forming the 4×4 mesh shown in fig. 9. The reinforcing beams were modeled with four quadratic beam elements, and the push rod and crank by three and two quadratic elements, respectively. In *case 2A*, the elastic component consisting of the panel and reinforcing beams was modeled by a modal based element featuring four boundary nodes at the four corners of the panel. Eight bending modes were used in the reduction, with boundary conditions corresponding to clamped conditions at points **A** and **D**. If the Craig-Bampton method had been used, it would have been required to use boundary conditions for the selected modes corresponding to clamped conditions at all boundary nodes, *i.e.* at points **A**, **B**, **C**, and **D**. With the proposed Herting transformation, arbitrary boundary conditions may be used, in particular those corresponding to clamped conditions at points **A** and **D** and free conditions at points **B** and **C** which are more representative of the deformation patterns expected to occur during operation. The body-attached frame was located at point **A**. In both cases, the crank period was set to $T = 0.2$ sec and a constant time step $\Delta t = 3 \times 10^{-04}$ sec was used in the simulations.

Cases 1B and *2B* are identical to *1A* and *2A*, respectively, except for the crank period which was reduced to $T = 0.05$ sec. A constant time step $\Delta t = 1 \times 10^{-04}$ sec was used.

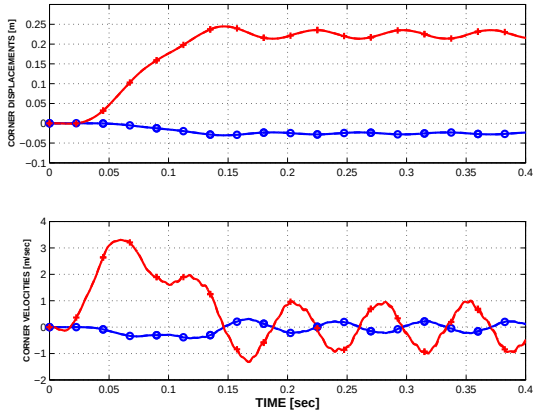

Figure 10: Time history of the vertical (+) and horizontal (∘) panel displacements (top graph) and velocities (bottom graph) at point **C** for *case 1A*: solid line and *case 2A*: dashed-dotted line.

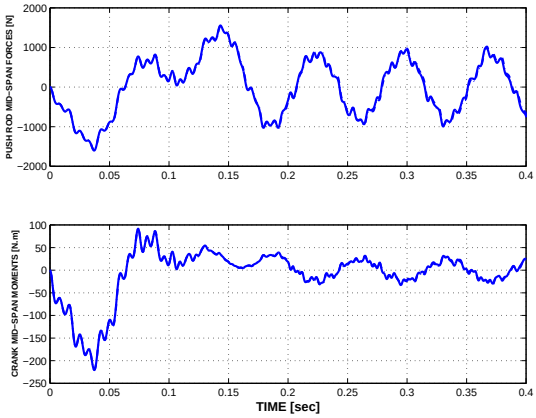

Figure 11: Time history of push rod mid-span axial force (top graph) and crank mid-span bending moment (bottom graph) for *case 1A*: solid line and *case 2A*: dashed-dotted line.

Fig. 10 shows the displacements and velocities of the panel at point **C** for *cases 1A* and *2A*. Excellent agreement is observed between the predictions of the full finite element and modal based simulations. Fig. 11 depicts the push rod mid-span axial force and crank mid-span bending moment. No appreciable differences are observed between the full finite element and modal based simulations. The full finite element simulation required about $1,750$ sec of CPU time compared to 16 sec for the modal based computation.

In the next set of simulations, the crank period was shortened to $T = 0.05$ sec. Due to the increased driving force, and system velocities and accelerations, the crank reached its final position more rapidly and nonlinear effects became more pronounced. Fig. 12 depicts the displacements and velocities of the panel at point **C** for *cases 1B* and *2B*. The full finite element and modal based simulations are in fair agreement during the early stages of the simulation, up to $t = 0.05$ sec. At this time, the crank reaches its final position $\phi = \pi/2$ rad and the discrepancies between the predictions of the two models become more pronounced. Fig. 13 depicts the push rod mid-span axial force and crank mid-span bending moment. The full finite element simulation predicts a 3,200 N.m peak-to-peak crank mid-span moment as compared to 2,100 N.m for the modal based approach, a 35% reduction. The required CPU times were $1,900$ and 16 sec for the full finite element and modal based simulations, respectively.

6 Conclusions

An approach to the modeling of modal based elements in nonlinear, flexible multibody systems has been presented. The proposed approach is based on Herting's transformation and presents attractive features. First, it allows the use of any modal basis the analyst sees fit. This contrasts with other approaches, such as those based on the Craig-Bampton of Rubin-MacNeal transformations that require specific boundary conditions for the selected modes. Second, the proposed approach can be used with a body-attached or moving frame; the body-attached frame was used in this work. Third, the modal based element is readily coupled to other components of the multibody system through the boundary nodes that retain physical degrees of freedom for this purpose. Fourth, the formulation recovers the exact equations of motion for a rigid body in the absence of elastic deformations.

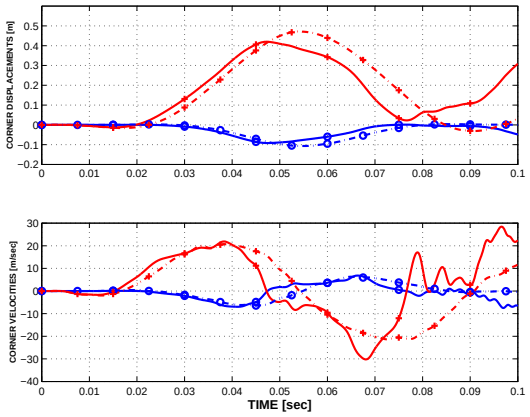

Figure 12: Time history of the vertical (+) and horizontal (∘) panel displacements (top graph) and velocities (bottom graph) at point **C** for *case 1B*: solid line and *case 2B*: dashed-dotted line.

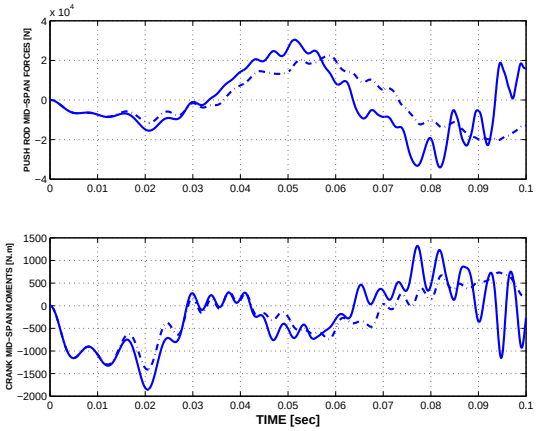

Figure 13: Time history of push rod mid-span axial force (top graph) and crank mid-span bending moment (bottom graph) for *case 1B*: solid line and *case 2B*: dashed-dotted line.

Finally, the proposed approach is completely independent of the finite element package used to compute the modes of the elastic components.

The numerical examples presented in this paper lead to the following observations. The selection of a suitable modal basis is a crucial step of the analysis that is eased by the versatility of the proposed approach. Modal based elements can be as accurate as their full finite element counterparts and can dramatically reduce computational times for complex multibody systems. It is important to validate the predictions of modal based elements against those of full finite element models. Indeed, erroneous results can be obtained if an inappropriate modal basis is used, or when nonlinear effects become appreciable, hence violating the basic assumptions of the modal based formulation.

References

[1] T.M. Wasfy and A.K. Noor. Computational strategies for flexible multibody systems. *ASME Applied Mechanics Reviews*, 56(2):553–613, 2003.

[2] A.A. Shabana. Flexible multibody dynamics: Review of past and recent developments. *Multibody System Dynamics*, 1(2):189–222, June 1997.

[3] O.P. Agrawal and A.A. Shabana. Dynamic analysis of multibody systems using component modes. *Computers & Structures*, 21(6):1303–1312, 1985.

[4] W.S. Yoo and E.J. Haug. Dynamics of articulated structures. Part I. Theory. *Journal of Structural Mechanics*, 14:105–126, 1986.

[5] W.S. Yoo and E.J. Haug. Dynamics of articulated structures. Part II. Computer implementation and applications. *Journal of Structural Mechanics*, 14:177–189, 1986.

[6] A. Cardona and M. Géradin. Modelling of superelements in mechanism analysis. *International Journal for Numerical Methods in Engineering*, 32:1565–1593, 1991.

[7] O. Friberg. A method for selecting deformation modes in flexible multibody dynamics. *International Journal for Numerical Methods in Engineering*, 32:1637–1655, 1991.

[8] A. Cardona and M. Géradin. A superelement formulation for mechanism analysis. *Computer Methods in Applied Mechanics and Engineering*, 100:1–29, 1992.

[9] A. Cardona. Superelements modelling in flexible multibody dynamics. *Multibody System Dynamics*, 4:245–266, 2000.

[10] A.A. Shabana. Substructure synthesis methods for dynamic analysis of multi-body systems. *Computers & Structures*, 20:737–744, 1985.

[11] O.P. Agrawal and A.A. Shabana. Application of deformable-body mean axis to flexible multibody system dynamics. *Computer Methods in Applied Mechanics and Engineering*, 56(2):217–245, 1986.

[12] A.A. Shabana. Resonance conditions and deformable body co-ordinate systems. *Journal of Sound and Vibration*, 192:389–398, 1996.

[13] P. Ravn. *Analysis and Synthesis of Planar Mechanical Systems Including Flexibility, Contact and Joint Clearance*. PhD thesis, Technical University of Denmark, 1998.

[14] L. Meirovitch. *Elements of Vibration Analysis*. McGraw-Hill Book Company, New York, 1975.

[15] J.A.C. Ambrósio and J.P.C. Gonçalves. Complex flexible multibody systems with application to vehicle dynamics. In Jorge A.C. Ambrósio and Werner O. Schiehlen, editors, *Advances in Computational Multibody Dynamics, IDMEC/IST, Lisbon, Portugal, Sept. 20-23, 1999*, pages 241–258, 1999.

[16] J.A.C. Ambrósio. Geometric and material nonlinear deformations in flexible multibody systems. In Jorge Ambrósio and Michal Kleiber, editors, *Proceedings of Computational Aspects of Nonlinear Structural Systems with Large Rigid Body Motion, NATO Advanced Research Workshop, Pultusk, Poland, July 2-7*, pages 91–115, 2000.

[17] R.R. Craig and M.C. Bampton. Coupling of substructures for dynamic analyses. *AIAA Journal*, 6:1313–1319, 1968.

[18] R.H. MacNeal. A hybrid method of component mode synthesis. *Computers & Structures*, 1(4):581–601, 1971.

[19] S. Rubin. Improved component-mode representation for structural dynamic analysis. *AIAA Journal*, 13:995–1006, 1975.

[20] D.N. Herting. A general purpose, multi-stage, component modal synthesis method. *Finite Elements in Analysis and Design*, 1:153–164, 1985.

[21] R.M. Hintz. Analytical methods in component modal synthesis. *AIAA Journal*, 13:1007–1016, 1975.

[22] R.R. Craig and C. Chang. Free-interface methods of substructure coupling for dynamic analysis. *AIAA Journal*, 14:1633–1635, 1976.

[23] W.S. Yoo and E.J. Haug. Dynamics of flexible mechanical systems using vibration and static correction modes. *Journal of Mechanisms, Transmissions, and Automation in Design*, 108:315–322, 1986.

[24] E.J. Wu, S. Haug. Geometric non-linear substructuring for dynamics of flexible mechanical elements. *International Journal for Numerical Methods in Engineering*, 26:2211–2226, 1988.

[25] A.A. Shabana and R.A. Wehage. A coordinate reduction technique for dynamic analysis of spatial substructures with large angular rotations. *Journal of Structural Mechanics*, 11(3):401–431, March 1983.

[26] K.J. Bathe. *Finite Element Procedures*. Prentice Hall, Inc., Englewood Cliffs, New Jersey, 1996.

[27] O.A. Bauchau. Computational schemes for flexible, nonlinear multi-body systems. *Multibody System Dynamics*, 2(2):169–225, 1998.

[28] O.A. Bauchau and C.L. Bottasso. On the design of energy preserving and decaying schemes for flexible, nonlinear multi-body systems. *Computer Methods in Applied Mechanics and Engineering*, 169(1-2):61–79, 1999.

[29] O.A. Bauchau, J.Y. Choi, and C.L. Bottasso. On the modeling of shells in multibody dynamics. *Multibody System Dynamics*, 8(4):459–489, 2002.